



Deformable Contour Method: A Constrained Optimization Approach

Xun Wang, Lei He, Chia Y. Han, William G. Wee
Electrical & Computer Engineering and Computer Science
Department

University of Cincinnati, Cincinnati, OH 45221

Xun_wang_2001@yahoo.com, lhe@ececs.uc.edu,
chia.han@uc.edu, wwee@ececs.uc.edu

Abstract

In this paper, a new deformable contour method derived from a constrained contour energy minimization framework is presented. By imposing a constraint of region, which can be any function characterizing features of the contour interior structures (including homogeneity, texture, and color, etc.), to boundary-based contour energy minimization, the method can incorporate a very general class of modeling information from both boundary and interior region. More favourable results comparing to the conventional deformable contour methods are demonstrated.

1 Introduction

Image segmentation is a fundamental issue in computer vision. As one of the most successful image segmentation techniques, deformable contour methods have received a tremendous amount of attention in a variety of areas, including robot vision, pattern recognition, and biomedical image processing. Typically, deformable contour methods model image segmentation as a contour energy minimization problem, which is dependent only on image gradient (boundary-based). In searching for the contour energy minimum, many approaches have been proposed [8]. A traditional difficulty with these approaches is that, due to the presence of other objects in an image and noise, there are numerous energy minima. Consequently, undesired contour energy minima, instead of target boundary, are often generated. As a solution, “balloon force” concept was brought up in [5], which tries to push the contour nearby the target boundary in order to locate it. This concept is extensively applied in later literatures [2], [14], [11]. But as “balloon” forces are functions of image gradient or constants, it can be still difficult for the balloon force to distinguish the neighborhood of target boundary from those of undesired contour energy minima, when image gradient information is either noisy or inaccurate in identifying target boundary. As an alternate solution to the problem of multiple contour energy minima, non-deterministic approaches [9], [6] search for a global contour energy minimum. The problem with these methods is that, in a complex image context, the target boundary is usually a local energy minimum. To make the target boundary be the global energy minimum, two conditions are often needed. Either a major



modification of energy function, incorporating specific prior knowledge on target boundary [9], or a preset mask [6] constraining the contour searching space within a neighborhood close to target boundary is required. Region-based deformable contour method is one way to avoid the problem of boundary-based methods, by considering boundary extraction as minimizing region-based energy functions [4], [12]. That means some prior knowledge of the region and image structure, such as the number and mean brightness of the objects in the image, is often required. Such information is not readily available in many implementations. Another problem is that these methods are only based on region features and may obtain inaccurate contours due to lack of image gradient information.

In this work, we focus on integrating region and boundary information into one framework. Specifically, our strategy is to add the region information to the existing boundary-based deformable contour formulation. Since region information is more global and less susceptible to noise, it will make the approach more robust and precise. We note here that in the literature of deformable contour methods, there have been work [15], [16] addressing this issue, and similar ideas have been proposed in other image segmentation methods as well, although with rather different natures [3], [7]. In [3], a model based boundary finder that integrates region and boundary information is presented. The method is robust to noise but has difficulty in handling complex shape and poor initialization. In [7], an original framework incorporating information from both region and boundary is proposed. However, this method still requires that the functions incorporating region information, or the integral of the region characterization function over the region, be expressed by an integral over its boundary.

This work takes the viewpoint that region information can be introduced as extra constraints within the contour energy minimization framework. With this in mind, the contour energy minimization problem is then formulated as searching for an energy minimum contour with its interior satisfying a constraint of region features. The constraint can be any function characterizing the contour interior structure, such as homogeneity, texture, and colour. The introduction of the constraint is to limit the contour searching in a subspace of contours with desirable interior properties, whereby undesirable local energy minima are eliminated and target boundaries are much easier to be located. To solve this constrained contour energy minimization problem, a new method derived from evolution strategy is developed. The method incorporates not only boundary features (by minimizing contour energy) but also a general class of modelling information from contour interior region (by imposing the constraint). As a special case, a constraint function based on region homogeneity inside the contour is proposed. The versatility and robustness of the method with this constraint is then evaluated by using challenging biomedical image applications where extracting contours with gaps, complex shapes, and interior noises are common requirements. High computational complexity due to energy minimization by evolution strategy is avoided by limiting the contour searching space within a small set of contour individuals. In many cases, the results outperform by far the conventional deformable contour methods.

The derivation of the proposed method and the algorithm description are introduced in Section 2 and Section 3, respectively. A brief comparison of the performance of the method with those of others is illustrated in Section 4. Finally, conclusions are contained in Section 5.

2 The Derivation of New Method



We formulate the problem as follows. We first start with boundary model.

Let Φ be an open domain subset of \mathfrak{R}^2 and $I(x, y): \Phi \rightarrow \mathfrak{R}$ be the image intensity function. Assume that target boundary $\Gamma(s) \subset \Phi$ is a closed contour with minimum energy,

$$E(\Gamma(s)) = \text{Min}E \quad (1)$$

where s is the parameter of $\Gamma(s)$ and $E(\cdot)$ is an energy function,

$$E(\Gamma(s)) = \frac{1}{\oint_{\Gamma(s)} ds} \left\{ \oint_{\Gamma(s)} \frac{1}{1 + |\nabla G * I(x(s), y(s))|^p} ds \right\} \quad (2)$$

where $p = 1$ or 2 , $|\nabla G * I|$ is the absolute value of the gradient of $I(x, y)$ smoothed by a Gaussian filter $N(0, \sigma^2)$. It should be noted that $E(\cdot)$ taking the form of Eq. (2) is not strictly necessary and can be replaced by energy functions such as of [8], [2].

Let region $\Omega_{\Gamma(s)}$ be the interior of $\Gamma(s)$. To characterize this region $\Omega_{\Gamma(s)}$, we assume that there exists a characteristic function $D(x, y)$ satisfying the following condition,

$$D(x, y) - T_v \geq 0 \quad \text{if } (x, y) \in \Omega_{\Gamma(s)} \quad (3)$$

where T_v is a given constant. $D(x, y)$ can be any arbitrary function of region features including colour and texture. From Eq. (3), a very general class of the modelling information from region can be incorporated into the contour energy minimization framework.

Considering all the difficulties associated with the various natures that exist in image segmentation problems, defining a general $D(x, y)$ that can be universally applied is a challenging task. In this paper, we bring up a $D(x, y)$ function that is based on the region homogeneity properties.

$$\text{Let } D(x, y) = A(x, y)B(x, y) \quad (4)$$

$$\text{with } A(x, y) = \frac{1}{1 + |\nabla G * I(x, y)|^2} \text{ and } B(x, y) = e^{-\frac{|I(x, y) - I_0|}{s}}.$$

where I_0 is the average intensity over region $\Omega_{\Gamma(s)}$. $A(x, y)$ represents a measurement of smoothness as a function of point gradient, and $B(x, y)$ is a measurement of smoothness as a potential function of deviation from an average brightness value I_0 of the interior region. Therefore, $D(x, y)$ as given in (4) can be considered as a homogeneity measure of smoothness at an interior point (x, y) . A large value of the gradient and a large deviation of the point brightness from I_0 produce a much smaller value of $D(x, y)$.

We are now ready to give the problem statement. Our problem is to find a closed contour $C(s, t)$ enclosing region Ω_c , such that

$$E(C(s, t)) = \frac{1}{\oint_C ds} \left\{ \oint_C \frac{1}{1 + |\nabla G * I(x(s), y(s))|^p} ds \right\} \quad (5)$$

is minimized with the constraint

$$D(x, y) = \frac{1}{1 + |\nabla G * I|^2} e^{-\frac{|I(x, y) - I_0|}{s}} \geq T_v \quad (6)$$

for all $(x, y) \in \Omega_c$.



Our solution to the constrained optimization problem is to use evolution strategy to deform $C(s, t)$ until an optimum is reached. The evolution strategy is to mimic the process of evolution, the deriving process for emergence of complex and well-adapted organic structure [1]. It is a recursive process in which a population of individuals, the parents, mutates and recombines to generate a large population of offspring. These offspring are then evaluated according to a fitness function and as a result, a best subset of offspring is selected to replace the existing parents. There are three main factors to consider:

1. The representation of individual contours – Individual contours are represented by states.
2. Variations of states – There are two types of state variation scheme: mutation and recombination. We consider the mutation as $C(s, t)$ varies by satisfying the constraint of Eq. (6), and mutates [1] by adding a Gaussian $\sigma_0 N(0,1)$ perturbation. The recombination of contours requires a much higher computational complexity and is not being currently used in our application.

Let $F(C(s, t)) = \iint_{\Omega_c} (D(x, y) - T_v) dx dy$. When the initial region interior of $C(s, 0)$

satisfies constraint Eq. (6), it can be proven that if $\frac{\partial F}{\partial t} \geq 0, t \geq 0$, then the interior of

$C(s, t)$ satisfies Eq. (6). To make $\frac{\partial F}{\partial t} \geq 0, t \geq 0$, with the analysis shown in the Appendix, the corresponding curve evolution formula is,

$$\frac{\partial C(s, t)}{\partial t} = (D(x, y) - T_v) \vec{N} \quad (7)$$

The contour driven by Eq. (7) grows outward when $D(x, y) > T_v$, and stops at points when $D(x, y) = T_v$. By incorporating the mutation process, we have

$$\frac{\partial C(s, t)}{\partial t} = [D(x(s, t), y(s, t)) - T_v - \mathbf{s}_0(s, t)N(0,1)] \vec{N}.$$

Let $\mathbf{s}_0(s, t) = tD(x, y)$ with $0 \leq t \leq 1$,

$$\frac{\partial C(s, t)}{\partial t} = [D(x, y)(1 - tN(0,1)) - T_v] \vec{N}$$

To reduce the point brightness noise contamination, in Eq. (6), $I(x, y)$ is replaced with a local average of size 3 by 3 denoted as $M(x, y)$. To further improve the efficiency of the mutation process is to let τ be a function depending on the local image brightness distribution as

$$t = Z_1 e^{-Z_1} \quad (8)$$

with $Z_1 = \frac{|I(x, y) - M(x, y)|}{\mathbf{s}_2}$ and $\mathbf{s}_2 = 2\mathbf{s}$.

The goal is to generate a velocity perturbation only when needed. For a small Z_1 indicating a rather smooth neighborhood, Eq. (8) produces a small τ to cause a small perturbation. For a large Z_1 indicating a rough neighborhood, also causes a small perturbation. Only when Z_1 is between these two extremes, the random perturbation is assigned a large value. Then we have

$$\frac{\partial C(s, t)}{\partial t} = \left[\frac{1}{1 + |\nabla G * I|^2} e^{-\frac{|M(x, y) - I_0|}{s}} (1 - tN(0,1)) - T_v \right] \vec{N} \quad (9).$$



3. Selection scheme – We apply a modified (m, I) selection scheme [1], where $m = \frac{N}{2}$ and $I = N$. The notation (m, I) indicates m parents create $I > m$ offspring by means of mutation, and the best m offspring individuals are deterministically selected to replace the parents. However, the acceptance of temporary deterioration might also make (m, I) selection drift away from the contour energy minimum. To avoid this, we select the state with the lowest energy from m survivors in (m, I) selection and compare it to the state of lowest energy selected from the previous selections. We save the state with lowest energy among all the selection processes as the output contour when the algorithm is over.

The described evolutionary method involves a contour evolution [10] formulation that maximizes an interior F function under perturbations so that the minimum E contour can be evaluated among the generated admissible contour set. The algorithm terminates under the following two conditions:

1. The maximum F is reached in less iterations than N_T and resulting minimum E contour is recorded as the solution.
2. The total number of iterations N_T has been reached and the resulting minimum E contour is recorded as the solution.

The resulting effect of the contour point velocity perturbation is equivalent to an adjustable T_v . Lowering T_v to zero makes N_T as the only stopping control. Therefore, the contour continues to expand with $D(\cdot) > 0$ for all image pixels and many local minimum E solutions are found in the process. To achieve the minimum E contour for a given T_v setting, the original level set [10] is needed which requires a much longer computation time while approximated solutions can be obtained in much less computation times using the fast marching approach [13]. An approximated solution is reached when the maximum contour point velocity (the maximum F is considered reached) is less than a preset velocity. A smaller T_v value produces a larger interior area that requires a larger iteration number in order to reach a boundary contour.

3 Algorithm Descriptions

As in many applications I_0 in Eq. (9) is not known, the method estimates I_0 using the region information of contour interior. Naturally, I_0 is estimated by $\hat{I}_0^{C(q,t)}$, the average intensity inside contour $C(q,t)$. Then the derived deformable contour algorithm is,

1. Input the Gaussian filtered image $I(x, y)$, initial interior location (x_0, y_0) , and parameters: \mathbf{s} (spreadness in $D(x, y)$), V_{th} (stopping velocity threshold), N_C (number of candidate contours), N_T (total number of iterations) and T_v .
2. Generate a contour around the 5 by 5 region centered at (x_0, y_0) ; duplicate another $(N_C - 1)$ copies; Fix $I_0 = \hat{I}_0^{C(q,0)}$, where $\hat{I}_0^{C(q,0)}$ is the average intensity inside the initial contour $C(q,0)$ and set the number of iterations to zero.
3. For each contour from the N_C contours performs the following:
 - i). Solve Eq. (9) using fast marching or level set method for 10 iteration
 - ii). Let $I_0 = \hat{I}_0^{C(q,t)}$ and fix it, where $\hat{I}_0^{C(q,t)}$ is the average intensity inside the current contour $C(q, t)$. Stop the whole process and record the minimum E contour as the



- solution, when the maximum point velocity is less than V_{th} , otherwise continue;
4. Compute E of Eq. (5) and select $N_C/2$ contours of the smallest E from the N_C contours; record the minimum E contour as a potential solution and its corresponding iteration number.
 5. Duplicate each contour of the selected $N_C/2$ contours once to constitute a set of new N_C contours; Stop the whole process when the number of iterations is larger than N_T , otherwise, go to Steps 3.
- The recorded minimum E contour is the solution contour.

4 Results and Comparison

Due to lack of space, in this paper, we can't present an extensive comparison of the method with the existing conventional deformable contour methods. We only show a simple comparison with four other methods to provide an indication of the efficiency of our approach. The first two methods are geodesic snakes [2], and area & length active contours [14] using $g(x, y) = \frac{1}{1 + |\nabla G * I|^2}$ as the edge detection function. The third

method is T-snake [11] and the fourth is GVF snake [17] with less than one hundred iterations to estimate its diffusion factors. The test image set contains two selected biomedical images and is shown in Fig. 4.1a and Fig. 4.2a with several initial contour locations added to each image. The initial positions are marked with either white dots on a dark background or dark dots on a light background. Fig. 4.2a is CT image of the stomach with additive noise of Gaussian noise (variance 3000). To conduct an objective evaluation, the variance of Gaussian filter of all the methods is set as the same value $\sigma_1 = 1$. In this evaluation, our task is to extract sulci contour in Fig. 4.1a and left kidney in Fig. 4.2a.

As shown in the following figures, the segmentation results using the proposed method has an obvious advantage over the conventional deformable contour methods¹.

The method has also been successfully applied in medical image data including visual blood cell images (Fig. 4.3). More results and detailed parameter settings can be found in [19].

5 Conclusions

We have introduced a framework of deformable contour methods based on constrained optimization. The framework can conveniently incorporate region features such as color, and texture. By limiting the contour searching space to a subset of contours with desirable interior features, the algorithm derived from the proposed framework is more robust to noises and in many cases, performs better than conventional deformable contour methods. In this paper, we have only used $D(x, y) = \frac{1}{1 + |\nabla G * I|^2} e^{-\frac{|I(x, y) - I_0|}{s}}$ to

¹ According to the evaluation by Professor Michael Behbehani of Molecular & Cell Physiology Dept. of University of Cincinnati, Dr. Nie and his colleagues in University of Kentucky hospital.



access the variation of contour interiors. This, however, does not constitute a limitation to the proposed method. In fact, our method can be easily extended to handle other measures of interior features, such as the similarity of color and texture [18]. It is also rather straightforward to incorporate shape information into $D(x, y)$ function. All these present a very desirable feature in many segmentation applications where the information from multiple sources is needed in a simple framework.

As for the computational complexity, it usually takes 30 seconds to 5 minutes for our algorithm to obtain most of the segmentation results in the ultra 10 Sun workstations. So the computational complexity is rather comparable to other deformable contour methods.

References

- [1] T. Buck, U. Hammel, and H. Schwefel, Evolutionary computation: comments on the history and current state. *IEEE Transaction on Evolutionary Computation*, Vol. 1, No. 1, pp. 3-17, 1997.
- [2] V. Casellas, R. Kimmel, and G. Sapiro, Geodesic active contours. *IJCV* Vol. 22, No. 1, pp. 61-79, 1997.
- [3] A. Chakraborty, James S. Duncan, Game-Theoretic Integration for Image Segmentation, *IEEE Trans. on PAMI*, Vol. 21, No. 1, pp. 12-30, 1999.
- [4] T. Chan, and L. Vese, Active Contours without Edges, *IEEE Trans on Image Processing*, Vol. 10, No. 2, pp. 266-277, 2001.
- [5] L. Cohen, On active contour models and balloons, *CVGIP: Image Understanding*. Vol. 52, No.2, pp. 211-218, March, 1991.
- [6] R. Grzeszczuk, and D. Levin, "Brownian String", Segmenting images with stochastically deformable contours. *IEEE Trans. on PAMI*, Vol. 19, No. 10, pp. 1100-1114, 1997.
- [7] I. Jermyn, and H. Ishikawa, Globally optimal regions and boundaries as minimum ratio weight cycles. *IEEE Transaction on Pattern Analysis and Machine Intelligence*, Vol. 23, No. 18, pp. 1075-1088, 2001.
- [8] M. Kass, A. Witkin, and D. Terzopoulos, Snakes: active contour models. *International Journal of Computer Vision*, Vol. 1, No.4, pp. 321-331, 1988
- [9] A. Lundervold, and G. Storvik, Segmentation of brain parenchyma and cerebrospinal fluid in multispectral magnetic resonance images. *IEEE Trans. on Medical Imaging*, Vol. 14, No.2, pp. 339-349, 1995.
- [10] R. Malladi, J. Sethian, and B. Vemuri, Shape Modeling with Front propagation. *IEEE Trans on PAMI*, Vol. 17, No.2, pp. 158-171, 1995.
- [11] T. McInerney, D. Terzopoulos, Topology adaptive deformable surfaces for medical image volume segmentation. *IEEE Trans on Medical Imaging*, Vol. 18, No.10, pp. 840-850, 1999.
- [12] C. Samson, L. Blanc-Feraud, G. Aubert, and J. Zerubia, A Level Set Model for Image Classification, *International Journal of Computer Vision*, Vol. 40, No. 3, pp. 187-197, 2000.
- [13] J. Sethian, A Fast Marching Level Set Method for Monotonically Advancing Fronts. *Proc. Nat. Acad. Sci.*, Vol. 93, No. 4, 1996.
- [14] K. Siddiqi, Y. B. Lauziere, A. Tannenbaum, S. W. Zucker, Area and length minimizing flows for shape segmentation, *IEEE Trans on Image Processing*., Vol. 7 pp 433-443, 1998.
- [15] X. Wang, and W. Wee, On a new deformable contour method, *IEEE International Conference on Image Analysis and Processing*, pp. 430-435, 1999.

- [16] X. Wang, L. He, and W. Wee, Constrained optimization: a geodesic snake approach, *International Conference of Image Processing 2002*. (accepted)
- [17] C. Xu, J. Prince, Snakes, shape, and gradient vector flow. *IEEE Trans. on Image Processing*. Vol. 7, pp. 359-369, 1998.
- [18] S. Zhu, A. Yuille, Region Competition: Unifying Snakes, Region Growing, and Bayes/MDL for Multiband Image Segmentation, *IEEE Trans. on PAMI*, Vol. 18, No.9, pp. 884-900, 1996.
- [19] X. Wang, L. He, and W. Wee, Deformable Contour Method: A Constrained Optimization Approach, submitted to *International Journal of Computer Vision*.

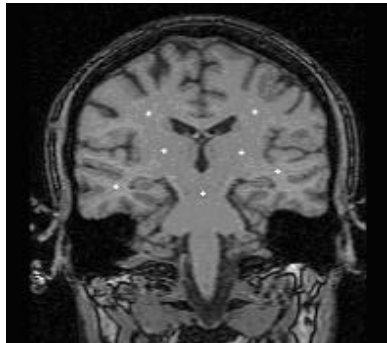


Fig. 4.1a Brain image

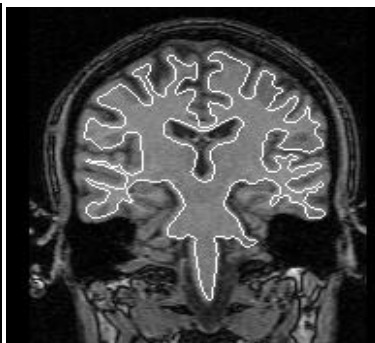


Fig. 4.1b Topology snake

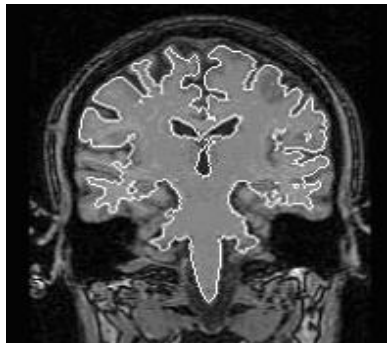


Fig. 4.1c Geodesic snake



Fig. 4.1d Area & Length active contour

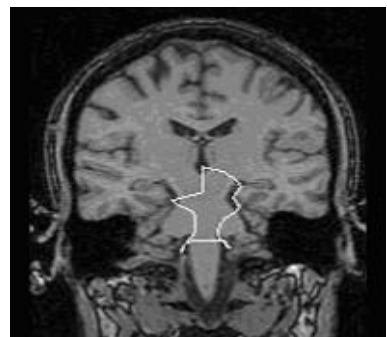


Fig. 4.1e GVF snake

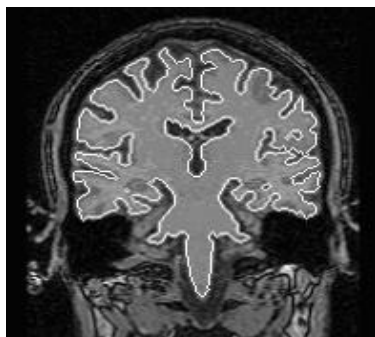


Fig. 4.1f Constrained optimization approach

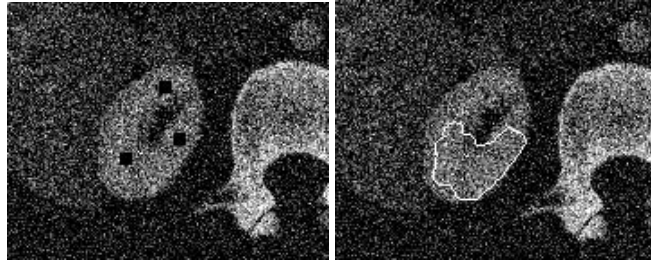


Fig. 4.2a Original image

Fig. 4.2b Topology snake

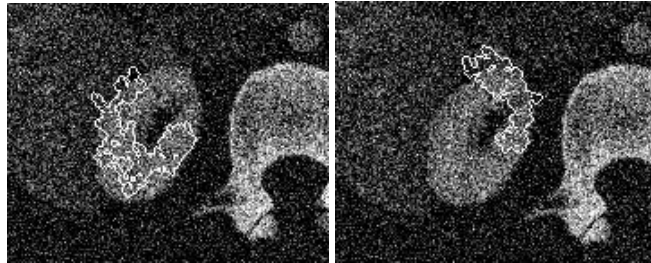


Fig. 4.2c Geodesic snake

Fig. 4.2d Area & length active contour

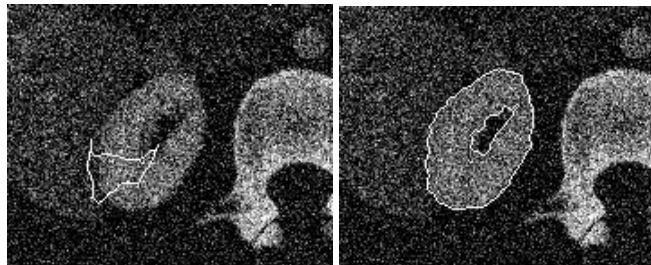


Fig. 4.2e GVF snake

Fig. 4.2f Constrained Optimization

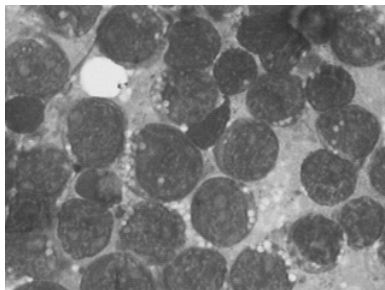


Fig. 4.3a Original cell image one

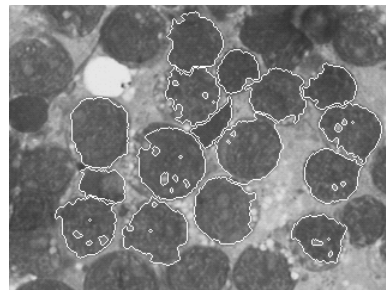


Fig. 4.3b Segmentation result of Fig. 4.3a

